

Effect of Composition and Surface Type on Activity of Transition Metal Oxides and Sulfides for CO₂ Electrochemical Reduction

Sahithi Ananthaneni^a, Rees B Rankin^{a,*}

^aChemical and Biological Engineering, Villanova University, White Hall, 800 E Lancaster Ave, Villanova University, Villanova, 19085, PA, USA

Abstract

Transition metal oxides (TMO) and transition metal sulfides (TMS) are proven to be promising electrocatalysts for CO₂RR but there is no clear understanding on catalyst activity or product selectivity based on trends in binding free energies. Therefore, a broader array of TMO and TMS are studied as electrocatalysts for CO₂RR thus addressing the gap in this field. This work shows how different types of surface facets with same catalyst composition can fine-tune the binding free energies of intermediate species by modifying the active binding site. Here, catalyst activity for CO₂RR towards formation of 4 different products is computed and compared for different materials with (100), (110) and (111) crystal facets and based on this, product selectivity is determined. Optimal catalyst design strategies for this family of materials are developed using the binding free energies of 4 key intermediate species COOH*, CO*, HCO* and H*. In this study, among the materials studied, ZnO zincblende (100) is the material that showed highest catalyst activity towards CO₂RR to CH₃OH and CH₄ while minimizing HER.

1. Introduction

Energy produced and consumed in various fields ranging from heating homes to manufacturing chemicals rely on fossil fuel usage, thereby increasing the concentration of carbon dioxide and other greenhouse gases in the atmosphere. Therefore, it is important to reduce and recycle the amount of carbon dioxide in the atmosphere. Recent advances in electrochemical reduction of CO₂ has opened many promising ways to convert into fuels and value-added chemicals. Despite several developments achieved in this field, it still faces few challenges (1) huge overpotential lowering the efficiency of the process, (2) poor product selectivity resulting in expensive separation processes [1–3]. It is well-known that the selectivity of products via electrochemical reduction of CO₂ primarily depends on the type of catalyst (electrode) material. In 1985, Hori *et al.* reported that among different transition

*Corresponding author.

Email address: rb.rankin@villanova.edu (Rees B Rankin)

metals, Cu is the only metal catalyst which can reduce CO_2 to value-added chemicals and additional experimental studies showed that CO_2 can produce 16 different products on Cu among which CH_4 and C_2H_4 have higher current densities. However, they still suffer from high overpotential of $\sim 1\text{V}$ and poor product selectivity. Many theoretical and experimental studies proposed that CO_2 reduction to desired products is primarily influenced by the binding strength of CO^* species (* indicates adsorbed species) which helped in providing a basis for designing various catalyst materials for CO_2RR (CO_2 reduction reaction) [4–6].

In our previous study on transition metal oxides and sulfides as electrocatalysts for CO_2 reduction, CO^* was hypothesized and determined to be the most suitable descriptor via scaling relations and a prototype volcano plot is achieved for CO_2 reduction to CH_3OH and CH_4 on TMO and TMS hybrid catalyst materials [7]. This plot presented that $\text{CO}_2 \rightarrow \text{COOH}^*$ and $\text{CO}^* \rightarrow \text{HCO}^*$ are the two intermediate reaction steps which define the catalyst activity for CO_2RR to CH_3OH and CH_4 . Since catalyst activity is affected by the binding energies of key intermediate species such as CO^* , the binding strength of these species can be altered by performing compositional and structural changes to catalyst materials. Inspired by the observations from our previous work, we study CO_2 reduction to CH_3OH and CH_4 as major products on a wide range of transition metal oxides and sulfides to understand how modifying active binding sites modify the catalytic efficiency. Typically, two approaches are followed: (1) increase the number of active sites by modifying catalyst surface for reaction to occur at different active sites, (2) increase the intrinsic activity of each active binding site by modifying its composition. Everywhere possible, we compare our methodologies and findings with those in other recent mechanistic studies involving CO_2 reduction reaction.

2. Methods

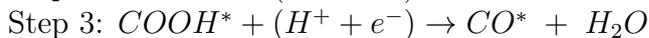
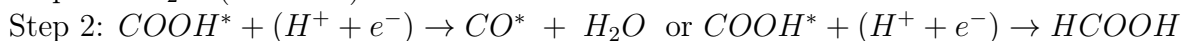
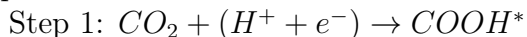
2.1. Theoretical calculations

In this work, we combine two strategies to select catalyst materials for CO_2 reduction. The first one is the use of electronegativity of transition metals as a factor to understand their catalytic nature due to their ability to adsorb and desorb from molecules [8]. Using the Pauling electronegativity scale, transition metals which are closer to the range of electronegative value of Cu are predicted to perform well as an electrocatalyst for CO_2RR . Another rational strategy for selection of catalysts and enhancing the catalytic performance is the tuning of electronic structure of electrocatalytic transition metals by introducing oxides or sulfides which has a different electronegative value than the transition metal. Because the binding properties of the adsorbate or intermediate species are determined by the electronic properties of the metal (catalyst), that is the nature of the d-band electrons, alloying the metal catalyst with another material is proven to be a powerful approach for designing and tuning CO_2RR catalyst materials [9–11]. Although alloying provides a direct approach to tuning the binding strength by modifying electronic structure, local structure also plays an important role for modifying catalyst activity [2]. The unique surface environment given by different types of crystal facets of a nanomaterial can control the nature of d-band electrons in a site-specific manner. Based on this idea, we study CO_2RR on transition metal oxides and sulfides given below and are arranged in the decreasing order of the electronegativity

of base metal and the materials considered in this study are thermodynamically stable form of W, Mo, Ag, Cu, Co, Zn, Mn oxides and sulfides with (100), (110) and (111) planar surfaces which is developed as a continuation of the previous work [7, 12, 13]. While our work is entirely computational, there are many encouraging experimental observations showing electrochemical CO₂ reduction through above mentioned transition metals and their alloys as electrocatalysts and guided us towards the selection of these metals with oxide and sulfide composition [14–20]. In specific, we study WO₃, MoO₃, Ag₂O, AgO, Ag₂S, CuO, Cu₂O, CuS, Cu₂S, Co₃O₄, ZnO, ZnS, MnO, MnO₂ for CO₂ reduction to four different products namely CO, HCOOH, CH₃OH and CH₄. Unit cell lattice parameters of each of these materials are given in supplementary information. Plane wave DFT calculations are performed on VASP to find optimized surface structures and calculate electronic structure properties [21–27]. These are performed using Van Der Waals, opt –PBE functional as they do not neglect dispersion forces with gamma centered k-points mesh of 2x2x1 and Fermi smearing of 0.2 eV is used. The convergence of ground state energies is set to less than 10⁻⁵eV/mole-unit cell with respect to k-point sampling. A vacuum space of 12 Å is defined to minimize the interactions between repeated slabs. Each intermediate is analyzed in top, bridge, FCC hollow and hcp hollow (wherever applicable) sites to find out the active site (the lowest energy formation site). All the reaction energy calculations are accomplished using the lowest energy conformation of the intermediate species with solvation effect into consideration. We have used implicit solvation model into the plane-wave DFT code throughout this work with water dielectric constant of 78.4 to describe the interactions between solute (intermediate species) and solvent (water).

2.2. Reaction network

In previous work a prototype volcano plot is achieved which shows that the two steps, CO₂ protonation and CO* protonation are the key intermediate steps which determine the catalyst activity and product selectivity i.e. if a particular catalyst material can reduce CO₂ to CH₃OH and CH₄ on TMO and TMS materials. The first three intermediate reaction steps in CO₂RR are shown below:

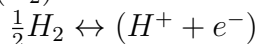


At step 2, based on the binding strength of CO*, the reaction can further proceed to form hydrocarbon fuels and value-added chemicals or can evolve as CO gas and depending on the binding free energies of formation of CO* and HCOOH, one product is preferred over the other. Binding energy of each adsorbate species is calculated by:

$$E_{binding} = E_{DFT} - (E_{surface} + x E_C + y E_H + z E_O)$$

E_{DFT} is the DFT energy of the intermediate species adsorbed onto the surface of the catalyst; $E_{surface}$ is the energy of the bare surface; E_C , E_H , and E_O are the energies of C, H, and O atom, respectively, calculated from gaseous CO, H₂, and H₂O. Using Norskov’s CHE method, free energies of formation of each of the reaction step along the reaction network are computed with RHE (reversible hydrogen electrode) as the reference electrode for all the reactions [28] Other reactions such as ORR, HER which involve proton-electron transfer

steps are also studied in the same fashion. Since it is tedious to computationally calculate the chemical potential of each proton-electron pair, we assume that protons and electrons are in equilibrium with one H₂ molecule at zero potential (U = 0), pH = 0, T = 300 K and P (H₂) = 1 ATM as shown below.



Binding free energy of formation of the first three steps in reaction network are calculated by:

$$\begin{aligned}\Delta G_{COOH^*} &= G_{COOH^*} - (G_{CO_2} + G_{0.5H_2}) \\ \Delta G_{CO^*} &= G_{CO^*} + G_{H_2O} - (G_{COOH^*} + G_{0.5H_2}) \\ \Delta G_{HCO^*} &= G_{HCO^*} - (G_{CO^*} + G_{0.5H_2})\end{aligned}$$

2.3. Screening based on binding free energies of CO*

Catalyst activity and product selectivity can be predicted by analyzing the binding free energies of descriptor on each of the catalyst material. From our previous studies on TMO and TMS materials as electrocatalysts for CO₂RR, we identified CO* as the descriptor using Sabatier's activity volcano plot. The binding free energy of CO* (descriptor) from this prototype volcano plot is -0.25 eV. Materials with stronger CO* binding free energies block the active sites of the surface of the catalyst and require higher over potential to further reduce to CH₃OH and CH₄. Those materials closer to the optimum binding free energies of CO* bind to the surface of the catalyst and are expected to further reduce to products with minimum theoretical overpotentials. Those materials with weaker binding free energies of CO* desorb immediately as gaseous CO as they are limited by the activation of reactants. As a first step towards screening, we calculate binding energies of CO* on all the materials considered in this study i.e. WO₃, MoO₃, Ag₂O, AgO, Ag₂S, CuO, Cu₂O, CuS, Cu₂S, Co₃O₄, ZnO, ZnS, MnO, MnO₂ with (100), (110) and (111) type of surfaces. From this pool, only those materials which showed binding free energy of CO* with a magnitude of 1.5 eV from the optimal binding free energy obtained from prototype volcano plot are studied. Those materials which fall away from the optimum binding energy range either due to too strong or too weak binding of CO* are eliminated.

3. Results and discussion

3.1. Scaling relations and volcano plots: CH₃OH and CH₄ as products

Scaling relations are obtained correlating binding free energies of CO* with COOH* and HCO* respectively for transition metal oxides and transition metal sulfide type of catalysts. These plots are shown in supplementary information. It is important to remember that CO* does not bind to single type of active binding site on all transition metal oxide and transition metal sulfide materials. Hence, it is common to have scatter in our scaling plots. If the materials have perfect linear scaling relations like in pure metals, then methane or methanol are the only products formed. Since our scaling relations have slight scatter, CO* is predicted to reduce a mixture of products at a certain reducing potential. That is, the competing reaction pathways in CO₂RR can generate a variety of chemically- similar bound

intermediates. These intermediates can form more than one product at a given reducing potential.

The binding free energy of formation of COOH* and HCO* intermediate species in the reaction network can be related to that of descriptor, CO* by the equations given below. These equations allow us to write limiting potential of each step as a function of CO* binding free energy.

$$\Delta G_{COOH^*} = -0.80 \Delta G_{CO^*} - 0.35 \text{ eV}$$

$$\Delta G_{HCO^*} = -0.97 \Delta G_{CO^*} - 0.03 \text{ eV}$$

As we know CO₂ → COOH* and CO* → HCO* are the two intermediate reaction steps which are potential limiting defining the catalyst activity, the above scaling relation equations are used to construct a comprehensive volcano plot comparing the activity of transition metal oxide and sulfide type of catalysts for CO₂RR. For a clear understanding, separate volcano plots for (100), (110) and (111) crystal facets are shown. Limiting/reducing potential of each catalyst material for CO₂ reduction to products is given by the corresponding y-axis value in the volcano plots. In Figures 1, 2 and 3 the difference between equilibrium potential of CH₃OH and CH₄ represented by dotted lines and reducing potential obtained for a catalyst material from the volcano shaped lines is the minimum theoretical overpotential required for reduction of CO₂ to CH₃OH or CH₄. CO* binding free energy at the peak of the volcano is defined as the optimum binding energy. The optimum ΔG(CO*) for the transition metal oxide and transition metal sulfide type of catalysts with low miller index surfaces is -0.28 eV. An important idea here is the optimum binding free energy of CO* from prototype volcano plot obtained in previous studies is -0.25 eV for six different materials with (100) type of crystal facet whereas the updated volcano plot displays optimum binding free energy of CO* as -0.28 eV for ten different materials with 3 different crystal facets. Comparing the optimum ΔG (CO*) from these two volcano plots, there has been a shift in the binding free energy of CO* towards left by only -0.03 eV. This means, addition of materials to the volcano plot will not qualitatively modify the conclusions reached based on the optimum binding free energy range of CO* but quantitatively there will be a slight shift in the peak of the volcano. This key result supports that this comprehensive volcano plot comparing the activity of a wide range of transition metal oxides and sulfides can be used as a basis to improve the activity of current catalysts or explore new catalysts for CO₂RR.

Those materials which have too strong CO* binding free energies require higher potentials for further reduction and those which have too weak binding free energies prefer CO_(g) as product. Since there are not enough experimental observations for all the materials studied here, there will be tiny amount of uncertainty on the predicted reducing potential and hence the activity. Therefore, an optimum binding free energy range is defined with a magnitude of ~0.3 eV w.r.t to optimum ΔG(CO*) and the materials that fall in this binding free energy range are predicted to show improved catalyst activity towards CO₂ reduction to CH₃OH and CH₄. These materials along with their descriptor, CO* binding free energies are tabulated below.

This table also shows how different surfaces of same catalyst composition can modify the reducing potential required for desired product formation based on how strong or ‘ the interactions of intermediates are with the surface of the catalyst. Modifying the surface type

Table 1: Materials in this study with maximum catalyst activity with their surface type and descriptor binding free energies are shown. Peak of the volcano is at $\Delta G(\text{CO}^*) = -0.28$ eV which is the optimum binding free energy of CO^* .

Catalyst material	Surface type	Active binding site	Descriptor $\Delta G(\text{CO}^*)$, eV	Reducing potential CO_2RR (V vs. RHE)	Experimental observations from literature (for comparison with results from current work)
ZnO zincblende	(100)	bridge	-0.13	-0.68	CO_2 reduction to CO on pristine ZnO occurs at reducing potential of -0.7 V vs. RHE. Studied up to CO as product [29].
	(111)	hollow	-0.15	-0.67	
MnO_2	(110)	bridge	-0.16	-0.66	CO_2 reduction is studied over MnO_2 nanosheets and CO starts forming at reducing potential of -0.7 V vs. RHE. Studied up to CO as product [30].
	(111)	top	-0.58	-0.85	
Ag_2O	(110)	bridge	-0.17	-0.66	CO_2 reduction is studied over Ag_2O and reduction occurs at potential of -1.0 V vs. RHE. Studied up to CO as product [31].
	(111)	top	-0.62	-0.88	
Cu_2O	(110)	bridge	-0.15	-0.67	CO_2 reduction on Cu oxides (110) to gaseous CO, CH_4 , C_2H_6 and C_2H_4 occurs at -1.1 V vs. RHE with minimum CO formation [32].
CuO	(110)	bridge	-0.04	-0.73	
CuS	(110)	top	-0.64	-0.90	CO_2 reduction to CO and CH_4 on CuO nanoarrays at potential -1.1 V vs. RHE [33].
ZnS zincblende	(111)	hollow	-0.22	-0.63	CO_2 reduction when studied over ZnS, CO is formed at reducing potential of -0.73 V vs. RHE [34].
	(111)	bridge	-0.14	-0.68	
MoO_3	(111)	bridge	-0.14	-0.68	No experimental results available
WO_3	(111)	top	-0.08	-0.71	No experimental results available

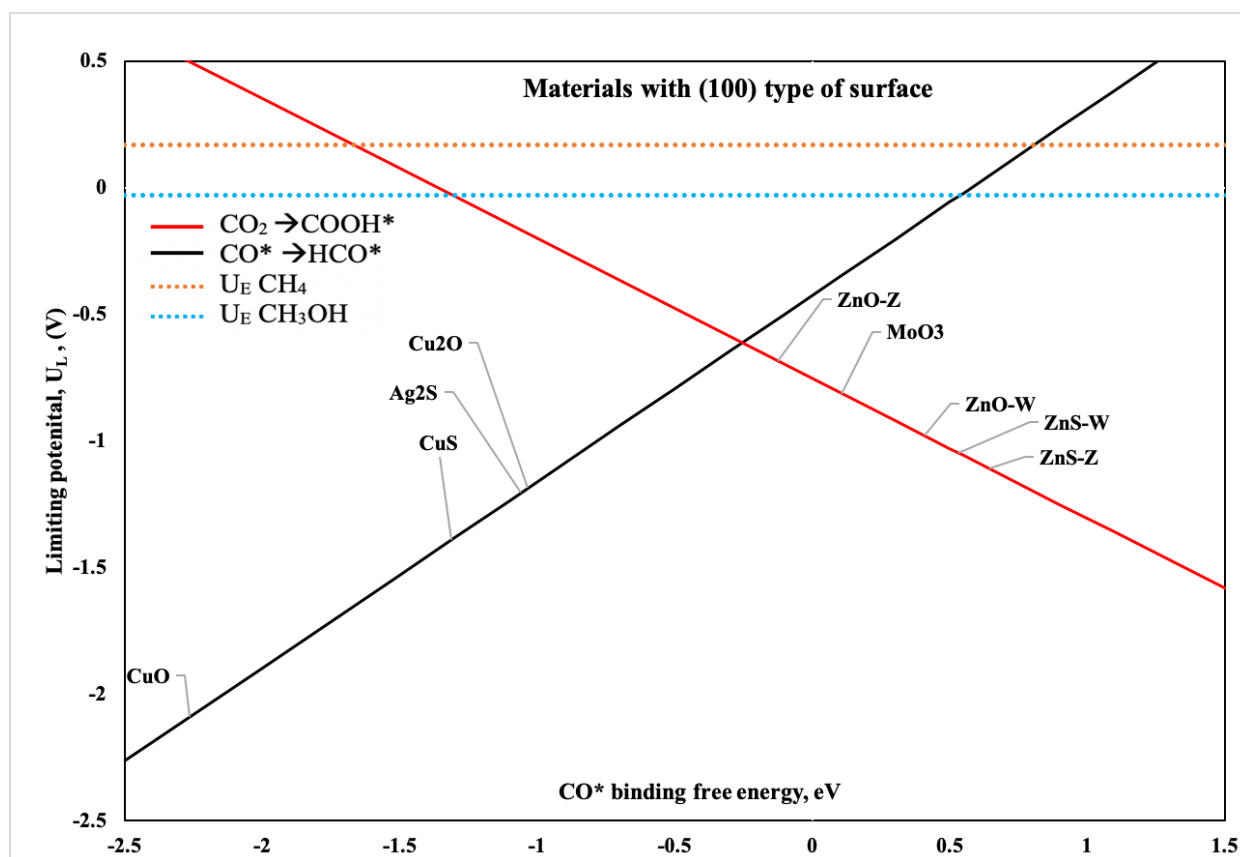


Figure 1: Volcano plot depicting catalyst activity of various materials in terms of limiting potential and CO^* binding free energy for materials with (100) type of surface

will fine-tune the binding free energies by modifying the active binding sites. For instance, MnO_2 (110) holds a descriptor binding free energy of -0.16 eV on bridge site whereas MnO_2 (111) holds a descriptor binding free energy of -0.58 eV on top site. Modifying the surface type modified the $\Delta G(\text{CO}^*)$ by ~ 0.4 eV. However, ZnO with (100) and (111) surfaces displays minor difference in binding free energies of descriptor and for this reason, the minimum reducing potential required for CO_2 reduction to C_1 products on ZnO (100) and (111) are similar. This table compares experimental observations from literature with the results from current work. There has been very limited study about overpotentials required for CO_2 reduction to CH_3OH and CH_4 on transition metal oxides and sulfides. As seen from the table, most of the theoretical and experimental studies on promising catalyst materials were conducted only up to CO formation, and CO_2 reduction to CH_3OH and CH_4 beyond Cu compositions is barely explored. This explains why current work on CO_2 RR via transition metal oxides and sulfides to CH_3OH and CH_4 is significant.

3.2. *HCOOH formation*

At the first proton electron transfer, CO_2 can either reduce to COOH^* or OCHO^* . From literature and our previous work on transition metal oxides and sulfides, if COOH^*

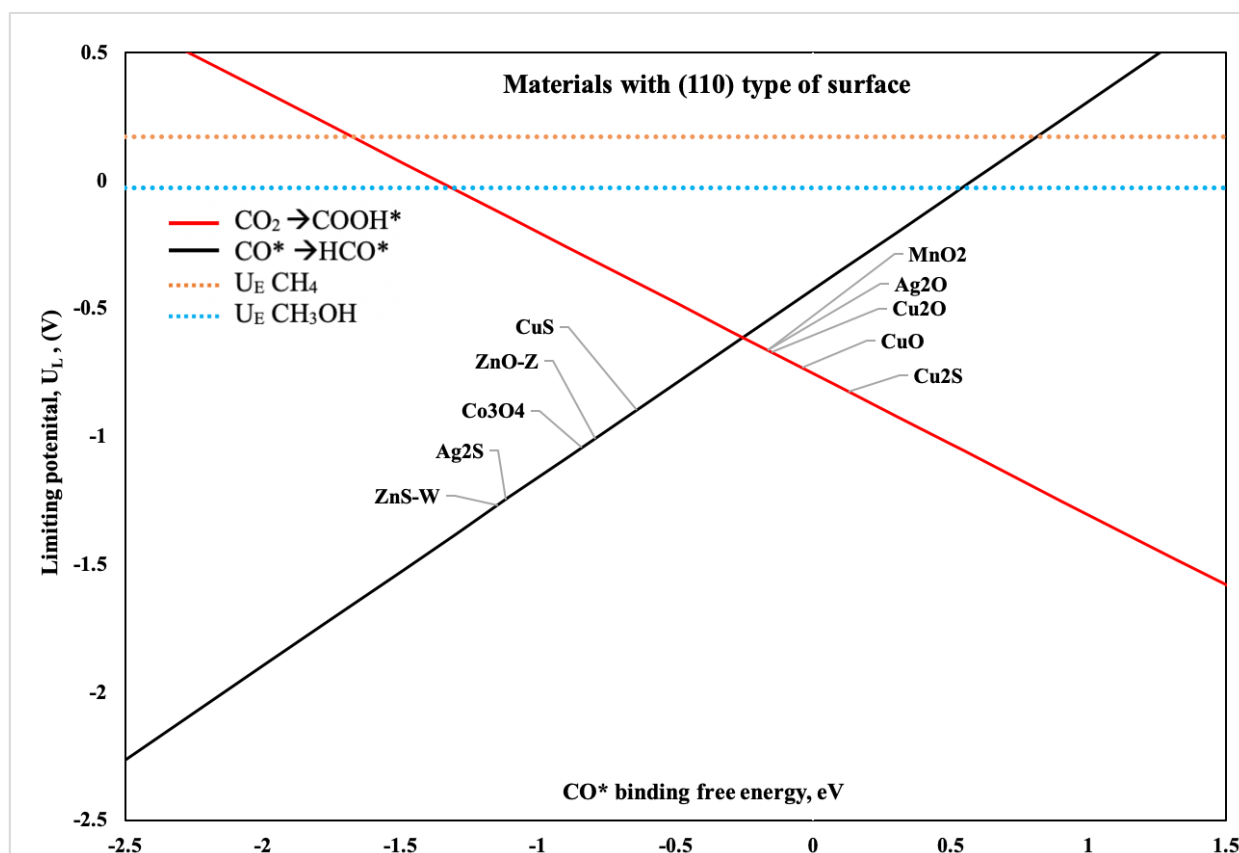


Figure 2: Volcano plot depicting catalyst activity of various materials in terms of limiting potential and CO^* binding free energy for materials with (110) type of surface

is preferred over OCHO^* for CO_2 reduction, the material favors CO , CH_3OH and CH_4 as products. However, if OCHO^* is preferred, the transition metal oxide catalysts show improved activity and selectivity towards HCOOH formation. All the materials selected in this study preferred COOH^* over OCHO^* , hence these are more favorable towards CO , CH_3OH and CH_4 formation at lower reducing potentials. Figure 4 compares reducing potential required for HCOOH formation on catalysts that showed highest activity towards CO_2RR in this study (presented in Table 1). This figure clearly shows HCOOH formation occurs at higher reducing potentials compared to CO_2 reduction to CO , CH_3OH and CH_4 formation (shown in Table 1). Based on this result it is confirmed that across different binding energy regime, among the pool of materials studied for current reduction reaction, the catalyst materials prefer COOH^* over OCHO^* and hence do not favor formic acid formation at low reducing potentials.

3.3. Design strategies for TMO and TMS electrocatalysts for CO_2RR

While the catalyst materials tabulated above showed better activity towards CO_2RR , it is important to understand hydrogen evolution reaction (HER) as thermodynamically both the reactions occur closer to 0V and H_2 formation is kinetically easy reaction to occur. Therefore,

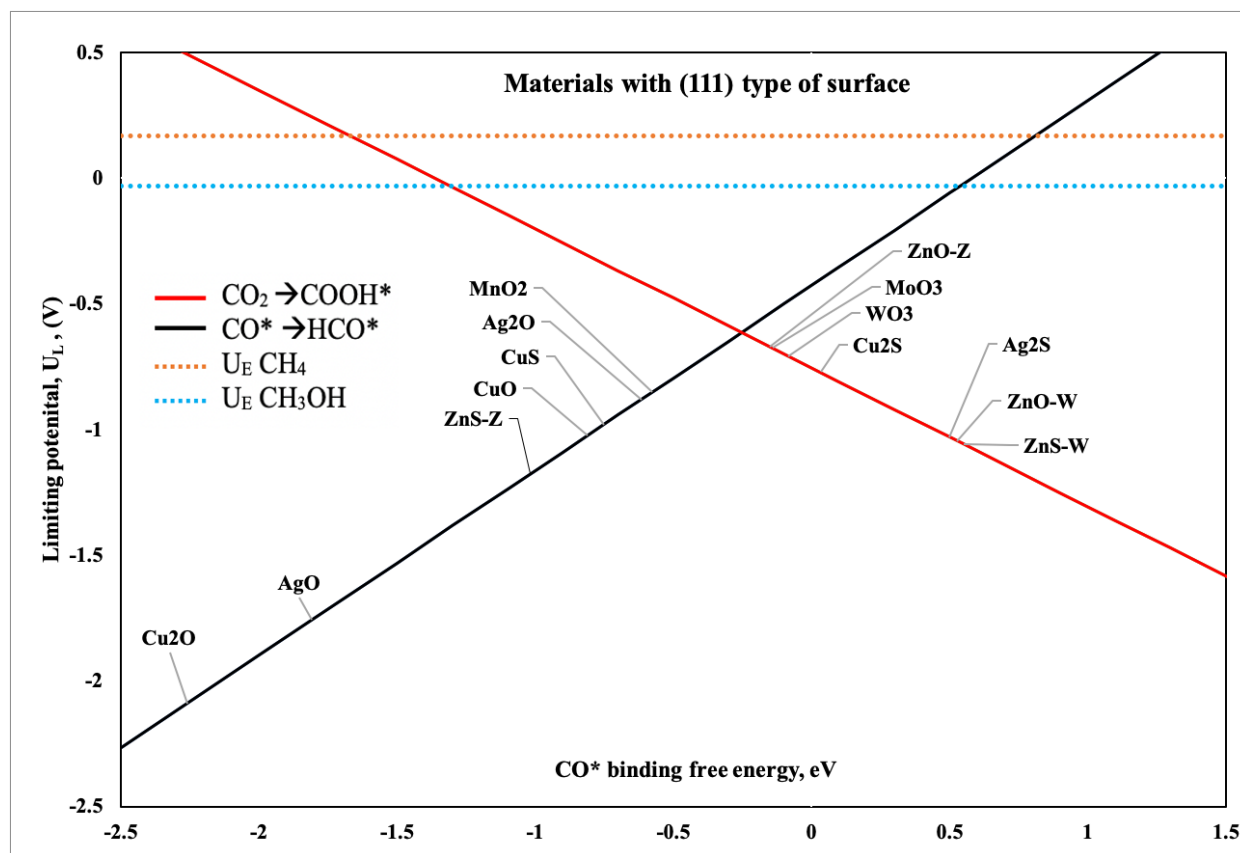


Figure 3: Volcano plot depicting catalyst activity of various materials in terms of limiting potential and CO^* binding free energy for materials with (111) type of surface

minimizing H_2 without compromising with the catalyst activity is a major challenge in CO_2 electroreduction process. In order to understand if CO_2 reduction is preferred over hydrogen evolution reaction (HER) on the catalysts systems without compromising with the product selectivity and catalyst activity, various design strategies are proposed which are mentioned below based on the results achieved so far. The design strategies adopted in this work are generally applicable towards designing other metal oxide and sulfide type of electrocatalysts or improving current catalyst systems for CO_2RR .

- COOH^* is supposed to bind stronger than H^* and at the same time COOH^* should bind weak enough to further reduce to CO^* at lower potential. Quantitatively, $\Delta G(\text{CO}^*) < \Delta G(\text{COOH}^*) < \Delta G(\text{H}^*)$.
- CO^* should bind to the surface within optimum binding free energy range and H^* should bind to the surface with positive binding free energy to limit $\text{CO}(\text{g})$ and $\text{H}_2(\text{g})$ formation and enhance CH_3OH and CH_4 formation.
- Reducing or limiting potential of $\Delta G(\text{CO}^*)$ formation step (y-axis value of volcano plots in Figure 1) should be minimum.

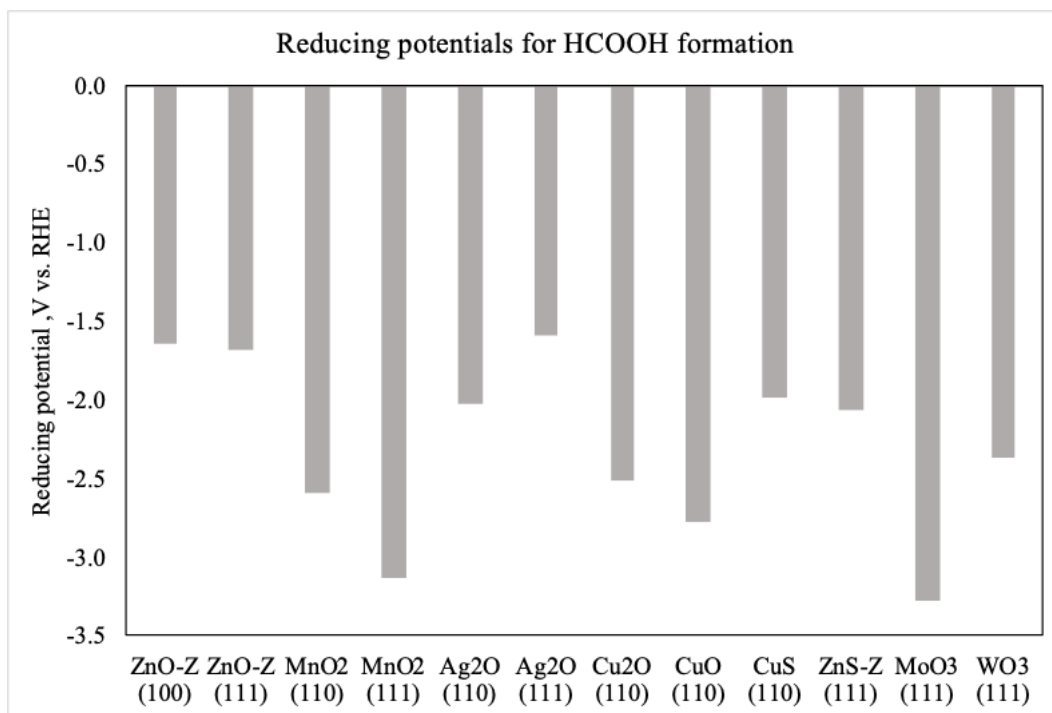


Figure 4: Comparison of reducing potential required for HCOOH formation on catalyst materials which showed highest activity towards CO₂ reduction to CO, CH₃OH and CH₄.

3.4. COOH* vs. H*

As the first proton-electron comes into contact with the reactant, CO₂ should form COOH* suppressing H₂ formation from H*. This happens when COOH* is more stable compared to H*. Simultaneously, COOH* should not bind too strong or the protonation of COOH* to form CO* will be too difficult favoring H₂ formation from H*. Figure 5 compares binding free energies of COOH* and H* intermediate species on different transition metal oxide and sulfide type of catalyst materials. The plot is divided into four quadrants based on the binding free energies of COOH* and H* and the materials which fall in green quadrant with weak COOH* and weak H* binding free energies show a promising area for CO₂ reduction to CH₃OH and CH₄. Among the materials which showed highest catalyst activity (from Table 1), those that fall in this region are ZnO zincblende (100), Ag₂O (111). The materials in red quadrant have strong COOH* and strong H* and the materials having either strong COOH* or strong H* are shown in blue quadrants and these materials although cannot reduce CO₂ at lower potentials by minimizing HER, they can be studied further by modifying the composition to improve their activity. The materials that fall in these regions with strong COOH* binding free energy region require high overpotentials for further reduction to products and those materials that fall within strong H* binding free energy region are favorable towards CO formation than further CO* reduction to CH₃OH and CH₄.

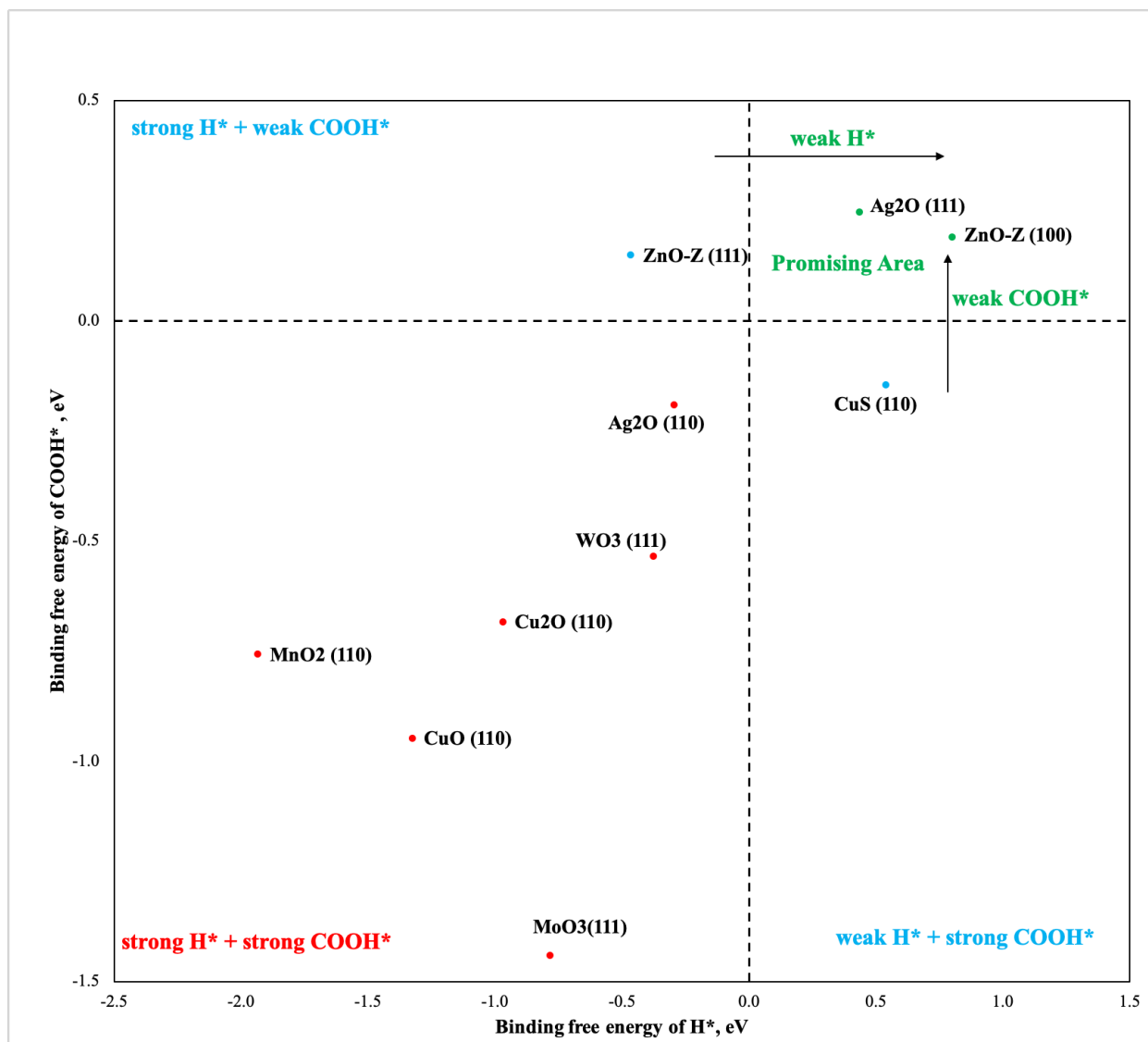


Figure 5: Binding free energies of COOH* vs H*intermediate species on transition metal oxide and sulfide type of catalyst materials which showed the highest activity among the pool of materials in our study. The plot is divided into 4 quadrants and the materials which fall in green quadrant with weak COOH* and weak H* binding free energies show a promising area for CO₂ reduction to CH₃OH and CH₄.

3.5. CO* vs. H*

The aim of our study is to convert CO₂ into CH₃OH and CH₄ on transition metal oxide and sulfide type of catalysts. To achieve this, CO_(g) and H_{2(g)} formation should be limited. Therefore, CO* must bind to the surface of the catalyst within optimum binding free energy range obtained from the volcano plot and H* should bind to the surface of the catalyst with positive binding free energy.

In Figure 4, CO* binding free energy is plotted as a function of the H* binding free energy to and all the materials considered in this study are divided into three categories

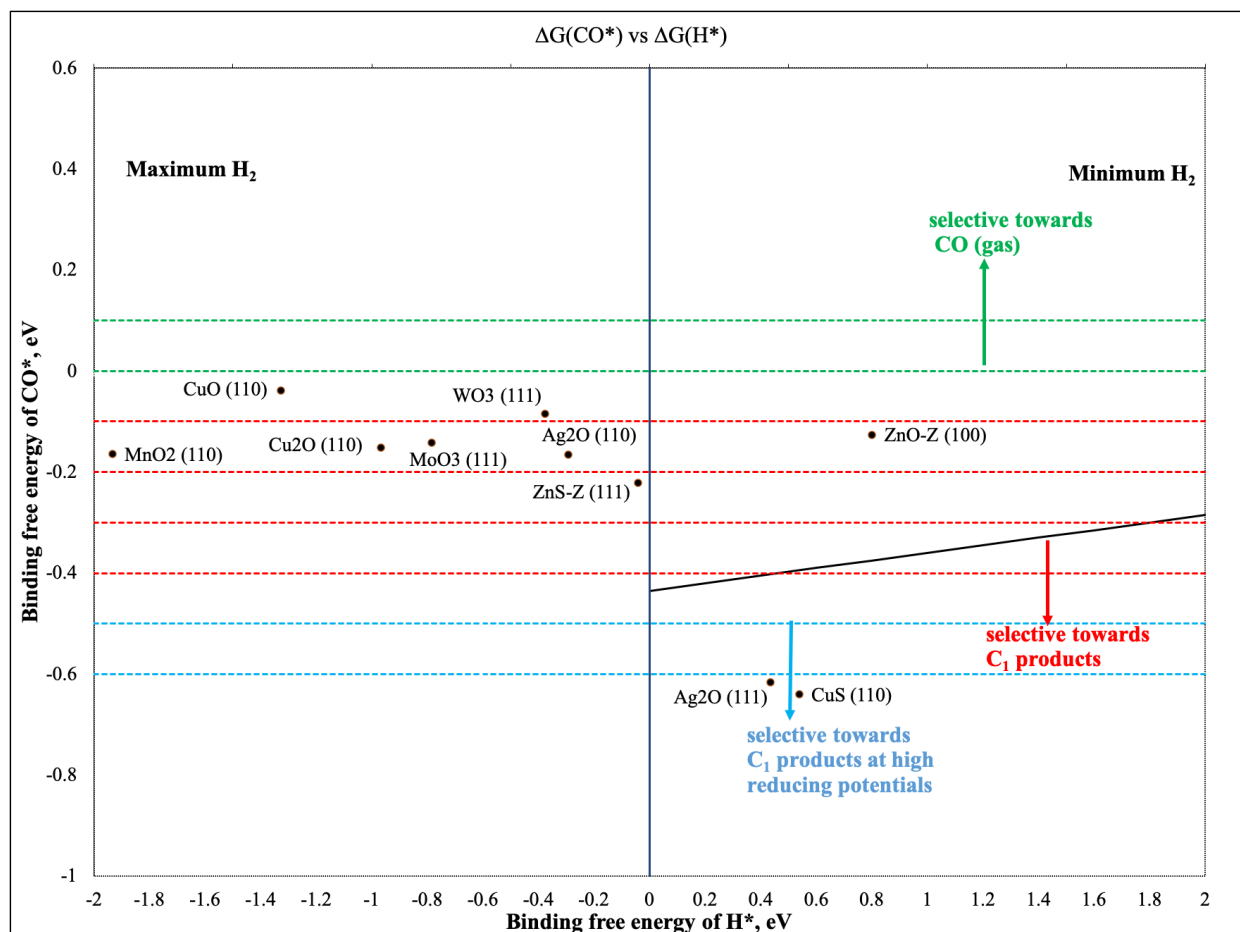


Figure 6: Linear relation between binding free energies of CO* and H*. Green dotted lines depict weak ΔG (CO*), blue dotted lines depict strong ΔG (CO*) region and red dotted lines depict optimum ΔG (CO*) region. Black solid line is the linear scaling line relating binding free energies of CO* and H*. Vertical blue solid line separates materials into two categories: strong (negative) H* binding free energy and weak (positive) H* binding free energies.

based on the product formed. Blue region shown in the figure is denoted as stronger binding free energy region of CO* and will cause further reduction of CO* but this occurs at higher overpotentials. Red binding free energy region in the figure is shown as the optimum binding free energy range and the materials that fall in this area are the promising materials in current study as these can further reduce to CH₃OH and CH₄ as products at lower reducing potentials. Weaker binding free energy region is shown by green region and materials in this region have weak ΔG (CO*) favoring CO_(g) formation with minimum amount of CH₃OH and CH₄. In the figure, materials towards the left of solid blue line at ΔG (H*) < 0 eV are selective towards C₁ products and H₂ because of strong (negative) H* binding free energy. Materials towards right of solid blue line i.e. ΔG (H*) > 0 eV are selective towards C₁ products while minimizing H₂ formation because of poor/positive H* binding free energies. Therefore, the materials that have positive H* binding free energy (right of black dotted

line) and falls in red binding free energy region are the most promising ones. Among the materials studied in this work, ZnO zincblende (100) is the material that satisfy this criterion and is located in this active and selective area. This is supported by findings from literature which shows that ZnO type of materials could be a potential catalyst for CO₂ reduction to CO at -0.62 V vs.RHE with Faradaic efficiency >90% [35].

It is important to understand that from volcano shaped activity plots achieved in Figures 1,2 and 3, ZnS zincblende (111) showed highest activity among the pool of materials studied in this work for CO₂RR. While combining this result with our design strategies and binding free energy analysis, this catalyst material has also proven to show decent activity towards HER. Since, the goal of an optimum catalyst for CO₂RR is to have increased catalyst activity towards formation of C₁ products as well as minimize HER, ZnO zincblende (100) is a promising catalyst for CO₂RR as this has shown higher catalyst activity towards CH₃OH and CH₄ formation simultaneously minimizing HER.

4. Conclusions

Transition metals as electrocatalysts has been extensively studied for CO₂RR, but the properties of metal oxides and metal sulfides, although shown to be potentially promising, are much less well understood. So far there haven't been any clear understanding of design rules or reaction mechanism trends for this family of electrocatalysts. In this work, a broader array of transition metal oxide (TMO) and transition metal-sulfides (TMS) electro-catalysts are studied as electrocatalysts for CO₂RR thus addressing the gap in this field. An in-depth understanding of CO₂ reduction to CH₃OH and CH₄ on TMO and TMS by constructing comprehensive volcano shaped activity plots which ranks the activity of catalysts based on descriptor (CO*) binding free energy is achieved. This work also demonstrated how different surfaces of same catalyst composition can fine-tune the binding free energies by modifying the active binding site. Catalyst activity for CO₂RR towards 4 different products is computed and compared for different materials with (100), (110) and (111) crystal facets. Optimal catalyst design strategies based on binding free energies of 4 important intermediate species COOH*, CO*, HCO* and H* are developed while dividing the catalysts into 3 categories based on the possibility of most favorable product formed on each surface: CO (gas) formation, C₁ products with minimum H₂ formation and just C₁ products but at higher reducing potentials. These strategies help in quick identification of possible good candidates for CO₂RR. In this work, binding free energy analysis shows there is a very specific and small region of space (green quadrant) with the most promising performance for CO₂RR and among the materials studied in this work, ZnO zincblende (100) is the material that falls in this quadrant and therefore is a promising catalyst towards CO₂RR to CH₃OH and CH₄ while minimizing HER. It is always possible to enhance the activity of this promising candidate by further modifying the composition either by creating oxygen vacancies or via single-element doping. All in all, this work aims to contribute to theoretical research on activity of transition metal/p-block materials especially transition metal oxide and sulfide type of materials.

Acknowledgments

R.B.R. gratefully acknowledges financial and research support from the Department of Chemical Engineering at Villanova University through his startup package fund. S.A. acknowledges financial support from the Department of Chemical Engineering and the College of Engineering at Villanova University as well. We acknowledge the Center for Nanoscale Materials, an Office of Science user facility, supported by the U.S. Department of Energy, Office of Science, Office of Basic Energy Sciences, under Contract no. DEAC02-06CH11357 for the use of Carbon cluster to perform calculations requiring high computing power and assistance from U.N.I.T. team at Villanova University for maintenance of computational resources necessary in this work.

References

- [1] S. Ma, P. J. Kenis, Electrochemical conversion of CO₂ to useful chemicals: current status, remaining challenges, and future opportunities, *Current Opinion in Chemical Engineering* 2 (2) (2013) 191–199.
- [2] W. J. Durand, A. A. Peterson, F. Studt, F. Abild-Pedersen, J. K. Nørskov, Structure effects on the energetics of the electrochemical reduction of CO₂ by copper surfaces, *Surface Science* 605 (15-16) (2011) 1354–1359.
- [3] M. Karamad, H. A. Hansen, J. Rossmeisl, J. K. Nørskov, Mechanistic pathway in the electrochemical reduction of CO₂ on RuO₂, *ACS Catalysis* 5 (7) (2015) 4075–4081.
- [4] M. R. Gonçalves, A. Gomes, J. Condeço, R. Fernandes, T. Pardal, C. A. C. Sequeira, J. B. Branco, Selective electrochemical conversion of CO₂ to C₂ hydrocarbons, *Energy conversion and management* 51 (1) (2010) 30–32.
- [5] Y. Hori, K. Kikuchi, S. Suzuki, Production of CO and CH₄ in electrochemical reduction of CO₂ at metal electrodes in aqueous hydrogencarbonate solution, *Chemistry Letters* 14 (11) (1985) 1695–1698.
- [6] K. P. Kuhl, E. R. Cave, D. N. Abram, T. F. Jaramillo, New insights into the electrochemical reduction of carbon dioxide on metallic copper surfaces, *Energy & Environmental Science* 5 (5) (2012) 7050–7059.
- [7] S. Ananthaneni, R. B. Rankin, Computational screening of transition metal/p-block hybrid electrocatalysts for CO₂ reduction, *Journal of Computational Chemistry* 41 (14) (2020) 1384–1394.
- [8] C. Nwosu, An electronegativity approach to catalytic performance, *Journal of Technical Science and Technologies* 1 (2) (2012) 25–28.
- [9] P. Hirunsit, W. Soodsawang, J. Limtrakul, CO₂ electrochemical reduction to methane and methanol on copper-based alloys: theoretical insight, *The Journal of Physical Chemistry C* 119 (15) (2015) 8238–8249.
- [10] J. He, N. J. Johnson, A. Huang, C. P. Berlinguette, Electrocatalytic alloys for CO₂ reduction, *ChemSusChem* 11 (1) (2018) 48–57.
- [11] Y. Wang, J. Liu, Y. Wang, A. M. Al-Enizi, G. Zheng, Tuning of CO₂ reduction selectivity on metal electrocatalysts, *Small* 13 (43) (2017) 1701809.
- [12] G. O. Larrazábal, A. J. Martín, F. Krumeich, R. Hauert, J. Pérez-Ramírez, Solvothermally-Prepared Cu₂O Electrocatalysts for CO₂ Reduction with Tunable Selectivity by the Introduction of p-Block Elements, *ChemSusChem* 10 (6) (2017) 1255–1265.
- [13] G. O. Larrazábal, A. J. Martín, J. Perez-Ramirez, Building blocks for high performance in electrocatalytic CO₂ reduction: materials, optimization strategies, and device engineering, *The journal of physical chemistry letters* 8 (16) (2017) 3933–3944.
- [14] H. Li, X. Liu, S. Chen, D. Yang, Q. Zhang, L. Song, H. Xiao, Q. Zhang, L. Gu, X. Wang, Edge-Exposed Molybdenum Disulfide with N-Doped Carbon Hybridization: A Hierarchical Hollow Electrocatalyst for Carbon Dioxide Reduction, *Advanced Energy Materials* 9 (18) (2019) 1900072.

- [15] D. Ren, J. Gao, S. M. Zakeeruddin, M. Grätzel, Bimetallic Electrocatalysts for Carbon Dioxide Reduction, *CHIMIA International Journal for Chemistry* 73 (11) (2019) 928–935.
- [16] W. Luo, J. Zhang, M. Li, A. Züttel, Boosting CO production in electrocatalytic CO₂ reduction on highly porous Zn catalysts, *ACS Catalysis* 9 (5) (2019) 3783–3791.
- [17] X. Peng, Y. Chen, Y. Mi, L. Zhuo, G. Qi, J. Ren, Y. Qiu, X. Liu, J. Luo, Efficient Electroreduction CO₂ to CO over MnO₂ Nanosheets, *Inorganic chemistry* 58 (14) (2019) 8910–8914.
- [18] W. Luc, C. Collins, S. Wang, H. Xin, K. He, Y. Kang, F. Jiao, Ag-Sn bimetallic catalyst with a core-shell structure for CO₂ reduction, *Journal of the American chemical society* 139 (5) (2017) 1885–1893.
- [19] S. Ananthaneni, Z. Smith, R. B. Rankin, Graphene Supported Tungsten Carbide as Catalyst for Electrochemical Reduction of CO₂, *Catalysts* 9 (7) (2019) 604.
- [20] X. Nie, W. Luo, M. J. Janik, A. Asthagiri, Reaction mechanisms of CO₂ electrochemical reduction on Cu (1 1 1) determined with density functional theory, *Journal of catalysis* 312 (2014) 108–122.
- [21] M. J. Piotrowski, C. G. Ungureanu, P. Tereshchuk, K. E. Batista, A. S. Chaves, D. Guedes-Sobrinho, J. L. D. Silva, Theoretical study of the structural, energetic, and electronic properties of 55-atom metal nanoclusters: A DFT investigation within van der Waals corrections, spin-orbit coupling, and PBE+U of 42 metal systems, *The Journal of Physical Chemistry C* 120 (50) (2016) 28844–28856.
- [22] S. Gautier, S. N. Steinmann, C. Michel, P. Fleurat-Lessard, P. Sautet, Molecular adsorption at Pt (111). How accurate are DFT functionals?, *Physical Chemistry Chemical Physics* 17 (43) (2015) 28921–28930.
- [23] J. Carrasco, J. Klimeš, A. Michaelides, The role of van der Waals forces in water adsorption on metals, *The Journal of chemical physics* 138 (2) (2013) 024708.
- [24] J. Hafner, Materials simulations using VASP—a quantum perspective to materials science, *Computer physics communications* 177 (1-2) (2007) 6–13.
- [25] T. Bucko, J. Hafner, S. Lebegue, J. G. Ángyán, Improved description of the structure of molecular and layered crystals: ab initio DFT calculations with van der Waals corrections, *The Journal of Physical Chemistry A* 114 (43) (2010) 11814–11824.
- [26] W. Koch, M. C. Holthausen, *A chemist’s guide to density functional theory*, John Wiley & Sons, 2015.
- [27] W. Kohn, A. D. Becke, R. G. Parr, Density functional theory of electronic structure, *The Journal of Physical Chemistry* 100 (31) (1996) 12974–12980.
- [28] A. A. Peterson, F. Abild-Pedersen, F. Studt, J. Rossmeisl, J. K. Nørskov, How copper catalyzes the electroreduction of carbon dioxide into hydrocarbon fuels, *Energy & Environmental Science* 3 (9) (2010) 1311–1315.
- [29] Z. Geng, X. Kong, W. Chen, H. Su, Y. Liu, F. Cai, G. Wang, J. Zeng, Oxygen vacancies in ZnO nanosheets enhance CO₂ electrochemical reduction to CO, *Angewandte Chemie International Edition* 57 (21) (2018) 6054–6059.
- [30] X. Peng, Y. Chen, Y. Mi, L. Zhuo, G. Qi, J. Ren, Y. Qiu, X. Liu, J. Luo, Efficient Electroreduction CO₂ to CO over MnO₂ Nanosheets, *Inorganic chemistry* 58 (14) (2019) 8910–8914.
- [31] M. Yang, J. Zhang, Y. Cao, M. Wu, K. Qian, Z. Zhang, H. Liu, J. Wang, W. Chen, W. Huang, Facet Sensitivity of Capping Ligand-Free Ag Crystals in CO₂ Electrochemical Reduction to CO, *ChemCatChem* 10 (22) (2018) 5128–5134.
- [32] R. Kas, R. Kortlever, A. Milbrat, M. T. Koper, G. Mul, J. Baltrusaitis, Electrochemical CO₂ reduction on Cu₂O-derived copper nanoparticles: controlling the catalytic selectivity of hydrocarbons, *Physical Chemistry Chemical Physics* 16 (24) (2014) 12194–12201.
- [33] Z. Zhao, X. Peng, X. Liu, X. Sun, J. Shi, L. Han, G. Li, J. Luo, Efficient and stable electroreduction of CO₂ to CH₄ on CuS nanosheet arrays, *Journal of Materials Chemistry A* 5 (38) (2017) 20239–20243.
- [34] C. Li, G. Shen, R. Zhang, D. Wu, C. Zou, T. Ling, H. Liu, C. Dong, X.-W. Du, Zn nanosheets coated with a ZnS subnanometer layer for effective and durable CO₂ reduction, *Journal of Materials Chemistry A* 7 (4) (2019) 1418–1423.
- [35] W. Luo, Q. Zhang, J. Zhang, E. Moioli, K. Zhao, A. Züttel, Electrochemical reconstruction of ZnO for selective reduction of CO₂ to CO, *Applied Catalysis B: Environmental* (2020) 119060.

Author biography

Rees B Rankin Assistant Professor

June 16, 2020